

# High Efficiency AC–AC Power Electronic Converter Applied to Domestic Induction Heating

Héctor Sarnago, *Member, IEEE*, Arturo Mediano, *Senior Member, IEEE*, and Óscar Lucia, *Member, IEEE*

**Abstract**—This paper presents the analysis and design of a new ac–ac resonant converter applied to domestic induction heating. The proposed topology, based on the half-bridge series resonant inverter, uses only two diodes to rectify the mains voltage. The proposed converter can operate with zero-voltage switching during both switch-on and switch-off transitions. Moreover, this topology doubles the output voltage, and therefore, the current in the load is reduced for the same output power. As a consequence, the converter efficiency is significantly improved. The analytical and simulation results have been verified by means of a 3600-W induction heating prototype. An efficiency study has been carried out, obtaining values higher than 96%.

**Index Terms**—Home appliances, induction heating, inverters, resonant power conversion.

## I. INTRODUCTION

INDUCTION heating appliance market is increasing due to its fastest heating time and efficiency. Domestic induction hobs are now becoming a standard option, especially in Asia and Europe.

The principle of operation is based on the generation of a variable magnetic field by means of a planar inductor below a metallic vessel [1], [2]. The mains voltage is rectified and after that an inverter provides a medium-frequency current to feed the inductor. The usual operating frequency is higher than 20 kHz to avoid the audible range and lower than 100 kHz to reduce switching losses. The most used device is the insulated gate bipolar transistor (IGBT) because of the operating frequency range and the output power range, up to 3 kW. Nowadays, most designs use the half-bridge series resonant topology because of its control simplicity and high efficiency [3]–[7].

In the past, several ac–ac topologies have been proposed to simplify the converter and improve the efficiency [8]–[10]. Considering the induction heating application, several resonant matrix converters featuring MOSFETs [11], [12], IGBTs [13], or RB-IGBTs [14], [15] have been proposed. However, the final

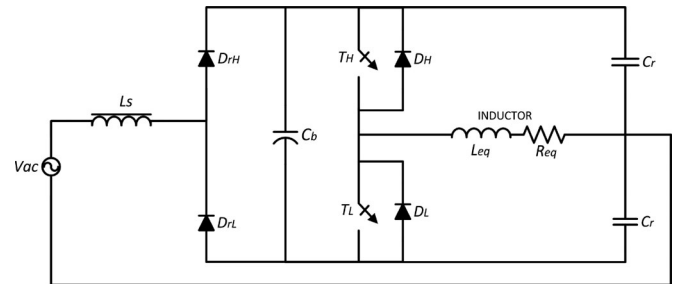


Fig. 1. Proposed ac–ac converter.

efficiency and cost are compromised due to the use of a higher number of switching devices. Other approaches, commonly used in electronic ballasts, simplify the rectifier stage in order to improve the converter performance [16]–[21]. This topology, known as half-bridge boost rectifier, reduces the switch count while keeping the same performance as more complex solutions.

The aim of this paper is to propose a new topology to improve the efficiency while reducing the power device count for induction heating applications. The proposed topology is based on the series resonant half-bridge topology and requires only two rectifier diodes. The effective output voltage is doubled, as in [22], [23], allowing a significant current reduction in the switching devices. Moreover, the proposed topology can operate with zero-voltage switching conditions during turn-on for both switching devices, and also during turn-off transitions for one of them. As a consequence, the efficiency is improved while the device count is reduced.

This paper is organized as follows. Section II describes the proposed topology. In Section III, a deeper analysis of the power converter is performed. Sections IV and V show the main simulation and experimental results, respectively. Finally, Section VI draws the main conclusions of this paper.

## II. PROPOSED POWER CONVERTER

The proposed topology (see Fig. 1) employs two bidirectional switches  $S_H$  and  $S_L$  composed of a transistor  $T_H$  or  $T_L$ , typically an IGBT, and an antiparallel diode  $D_H$  or  $D_L$ , respectively. The mains voltage  $v_{ac}$  is rectified by two diodes  $D_{rH}$  and  $D_{rL}$ , but only one of them is activated at the same time. This operation increases efficiency with regard to classical topologies based on a full-bridge diode rectifier plus a dc-link inverter.

The proposed topology is a series–parallel resonant converter. The inductor–pot system is modeled as an equivalent series resistance  $R_{eq}$  and inductance  $L_{eq}$ , as shown in Fig. 1 [24].

Manuscript received June 8, 2011; revised September 7, 2011 and November 14, 2011; accepted January 14, 2012. Date of current version April 20, 2012. This work was supported in part by the Spanish Ministerio de Ciencia e Innovación under Project TEC2010-19207, Project CSD2009-00046, and Project IPT-2011-1158-920000 and in part by the Bosch and Siemens Home Appliances Group under Grant PTAUZ-2011-TEC-A-004. Recommended for publication by Associate Editor L. M. Tolbert.

The authors are with the Department of Electronic Engineering and Communications, University of Zaragoza, Zaragoza 50009, Spain (e-mail: hsarnago@unizar.es; amediano@unizar.es; olucia@unizar.es).

Color versions of one or more of the figures in this paper are available online at <http://ieeexplore.ieee.org>.

Digital Object Identifier 10.1109/TPEL.2012.2185067

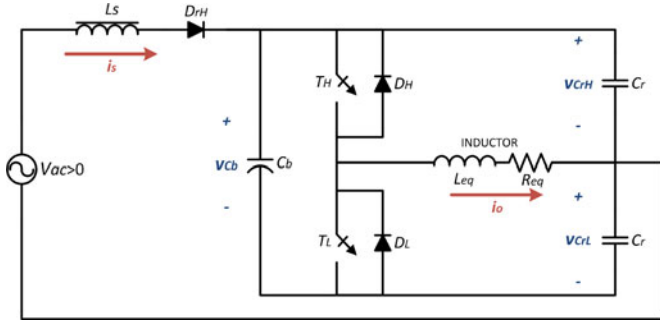


Fig. 2. Equivalent circuit during the positive mains voltage cycle.

This topology implements resonant capacitors  $C_r$  and may use a bus capacitor  $C_b$ . Due to the symmetry between positive and negative mains voltage, both resonant capacitors have the same value. An input inductor  $L_s$  is used to reduce the harmonic content to fulfill the electromagnetic compatibility regulations.

### III. ANALYSIS

The topology presents symmetry between positive and negative ac voltage supply. Its symmetry simplifies analysis and makes possible to redraw the circuit as shown in Fig. 2.

Although this topology uses different resonant configurations, parallel and series, and different resonant tanks for each of them, it is possible to use a normalized nomenclature based on series resonance

$$C_b = \alpha \cdot C_r, \quad \alpha \geq 0 \quad (1)$$

$$L_s = \beta \cdot L_{eq}, \quad \beta \geq 1 \quad (2)$$

$$\omega_0 = \frac{1}{\sqrt{L_{eq} \cdot C_r}} \quad (3)$$

$$\omega_n = \frac{\omega_{sw}}{\omega_0} \quad (4)$$

$$Z_0 = \sqrt{\frac{L_{eq}}{C_r}} \quad (5)$$

$$R_{eq} = \frac{\omega_0 \cdot L_{eq}}{Q_{eq}} = \frac{Z_0}{Q_{eq}} \quad (6)$$

where  $\alpha$  is the ratio between the dc-link and the resonant capacitors and  $\beta$  is the ratio between the input choke and the equivalent inductance of the inductor-pot system. The parameters  $\{\omega_0, \omega_{sw}, \omega_n\}$  are the angular resonant frequency, the angular switching frequency, and the normalized angular switching frequency, respectively.  $Z_0$  defines the equivalent impedance of the resonant circuit, defined by  $L_{eq}$  and  $C_r$ . Finally,  $Q_{eq}$  is the equivalent inductor-pot system quality factor at the resonant frequency. The system will be analyzed using the state-space description. Each state is completely defined by a differential equation system and the global system response is the conduction angle,  $\theta$ , average response of each state (I-III):

$$\dot{\mathbf{x}}(\theta) = \mathbf{A}_k \mathbf{x}(\theta) + \mathbf{B}_k \cdot v_{ac}, \quad k = \{1, 2, 3\}, \quad \theta = 0 \dots 2\pi \quad (7)$$

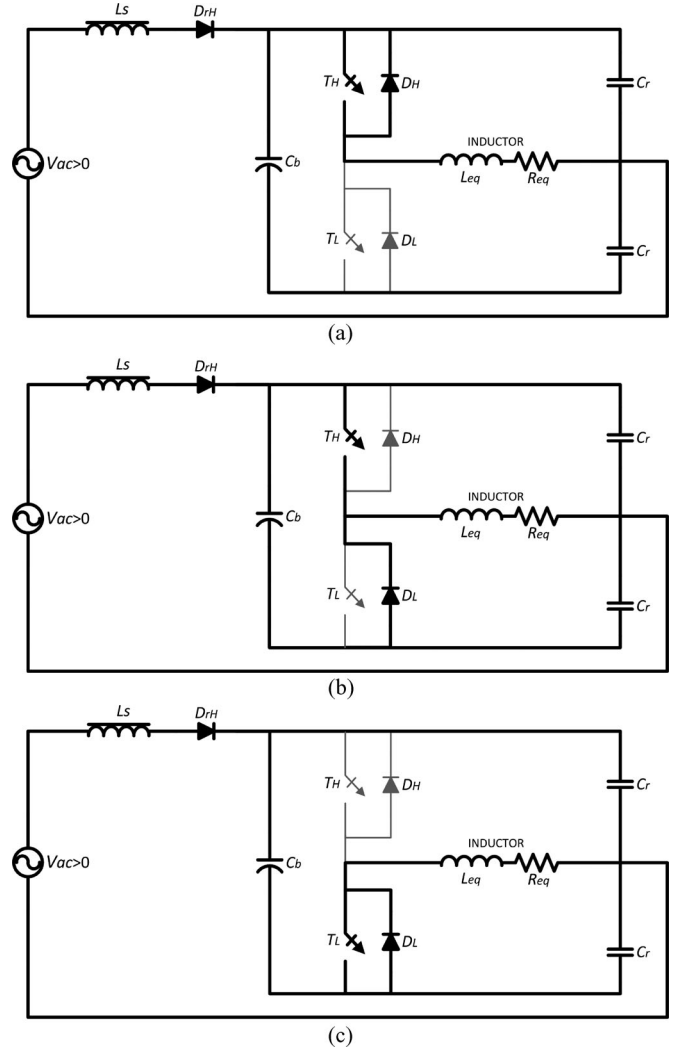


Fig. 3. Equivalent circuits. (a) State I, (b) state II, and (c) state III.

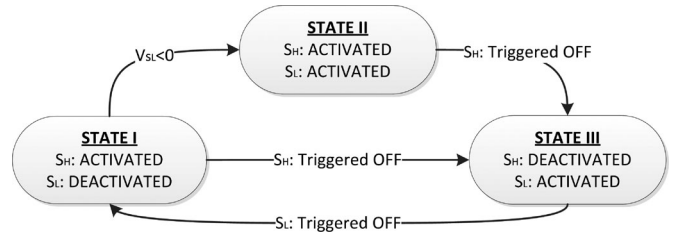


Fig. 4. States and transition conditions.

where the state variables  $\mathbf{x} = [i_s, v_{Cb}, v_{CrH}, v_{CrL}, i_o]^T$  are the input current, the voltage across the bus capacitor  $C_b$ , the voltage across both resonant capacitors, and the current through the load, respectively.

As is shown in Fig. 3, working under ZVS conditions, there are three different states. Each one has its characteristic differential equation system. Fig. 4 shows the transition conditions for each state.

State I operates with the high-side switching device  $S_H$  triggered-on and activated and the low-side switching device

( $S_L$ ) triggered-off. The parallel resonant circuit is set by an equivalent capacitor  $C_{eq}$ , obtained from  $C_r$  and  $C_b$  and expressed in (8), and the inductor electrical parameters,  $R_{eq}$  and  $L_{eq}$ . The current flowing through  $S_H$  is the same as the one flowing through the load

$$C_{eq} = C_r \left( 1 + \frac{C_b}{C_r + C_b} \right) = C_r \left( \frac{1 + 2\alpha}{1 + \alpha} \right). \quad (8)$$

State I begins when  $S_L$  is triggered OFF. In this moment, the antiparallel diode  $D_H$  conducts and  $S_H$  can be triggered ON ensuring ZVS switching-on conditions. Transitions from this state can lead either to state II or state III. If voltage across  $S_L$  reaches zero and  $D_L$  starts conducting, the transition condition to state II is fulfilled. On the other hand, if  $S_H$  is switched OFF when  $T_H$  conducts, the next state is state III.

The normalized differential equations that define the dynamics of the system in this state are

$$\frac{di_0(\theta)}{d\theta} = \frac{1}{\omega_n Z_0} (v_{C_{eq}}(\theta) - R_{eq} \cdot i_0(\theta)) \quad (9)$$

$$\frac{dv_{C_{eq}}(\theta)}{d\theta} = \frac{Z_0(1+\alpha)}{\omega_n(1+2\alpha)} (i_s(\theta) + i_0(\theta)) \quad (10)$$

$$\frac{di_s(\theta)}{d\theta} = \frac{1}{\beta\omega_n Z_0} (v_{ac} - v_{C_{eq}}(\theta)). \quad (11)$$

Therefore, the state-space matrices for state I are

$$\mathbf{A}_1 = \begin{pmatrix} 0 & 0 & \frac{-1}{\beta\omega_n Z_0} & 0 & 0 \\ \frac{Z_0}{\omega_n(1+2\alpha)} & 0 & 0 & 0 & \frac{Z_0}{\omega_n(1+2\alpha)} \\ \frac{Z_0(1+\alpha)}{\omega_n(1+2\alpha)\alpha} & 0 & 0 & 0 & \frac{Z_0(1+\alpha)}{\omega_n(1+2\alpha)\alpha} \\ \frac{-\alpha Z_0}{\omega_n(1+2\alpha)} & 0 & 0 & 0 & \frac{-\alpha Z_0}{\omega_n(1+2\alpha)} \\ 0 & \frac{1}{\omega_n Z_0} & 0 & 0 & \frac{-R_{eq}}{\omega_n Z_0} \end{pmatrix}$$

$$\mathbf{B}_1 = \begin{pmatrix} 1 \\ \frac{1}{\beta\omega_n Z_0} \\ 0 \\ 0 \\ 0 \\ 0 \end{pmatrix}. \quad (12)$$

State II is characterized by the conduction of both switching devices, although only  $S_H$  is triggered ON. That is,  $T_H$  and  $D_L$  conduct at the same time. Current through load is supplied by both devices ( $T_H$  and  $D_L$ ), and consequently, low conduction stress for the devices is achieved. The equivalent parallel resonant circuit is set by the inductor electrical parameters in parallel with both resonant capacitors.  $C_b$  is short-circuited by both switching devices. This state starts when the voltage across  $S_L$  reaches zero. At this moment,  $D_L$  starts conducting at the same time as  $T_H$  is triggered ON. This state finishes when  $S_H$  is triggered OFF and the next state is state III. The main benefit results of the lower switch-off current achieved when  $S_H$  is triggered

OFF, due to the fact that the load current is supplied by both devices. In addition,  $S_H$  achieves ZVS conditions during both switch-on and switch-off transitions, reducing consequently the switching losses.

The normalized differential equations that define the dynamics of the system in this state are

$$\frac{di_s(\theta)}{d\theta} = \frac{1}{\beta\omega_n Z_0} (V_s - v_{C_{rH}}(\theta)) \quad (13)$$

$$v_{C_b} = 0 \quad (14)$$

$$\frac{dv_{C_{rH}}(\theta)}{d\theta} = \frac{Z_0}{2\omega_n} (i_s(\theta) + i_0(\theta)) \quad (15)$$

$$\frac{dv_{C_{rL}}(\theta)}{d\theta} = \frac{-Z_0}{2\omega_n} (i_s(\theta) + i_0(\theta)) \quad (16)$$

$$\frac{di_0(\theta)}{d\theta} = \frac{1}{\omega_n Z_0} (v_{C_{rH}}(\theta) - R_{eq} \cdot i_0(\theta)). \quad (17)$$

The state-space matrix for this state is shown in the next equation

$$\mathbf{A}_2 = \begin{pmatrix} 0 & 0 & \frac{-1}{\beta\omega_n Z_0} & 0 & 0 \\ 0 & 0 & 0 & 0 & 0 \\ \frac{Z_0}{2\omega_n} & 0 & 0 & 0 & \frac{Z_0}{2\omega_n} \\ \frac{-Z_0}{2\omega_n} & 0 & 0 & 0 & \frac{-Z_0}{2\omega_n} \\ 0 & 0 & \frac{1}{\omega_n Z_0} & 0 & \frac{-R_{eq}}{\omega_n Z_0} \end{pmatrix}$$

$$\mathbf{B}_2 = \begin{pmatrix} 1 \\ \frac{1}{\beta\omega_n Z_0} \\ 0 \\ 0 \\ 0 \\ 0 \end{pmatrix}. \quad (18)$$

State III is defined by the conduction of  $S_L$  while  $S_H$  is deactivated. The equivalent resonant circuit is set by one resonant capacitor in parallel with the series connection of the  $C_b$  capacitor and the parallel connection of the inductor and the other one resonant capacitance. Note that when  $C_b$  is zero ( $\alpha = 0$ ), the equivalent resonant circuit is a series RLC circuit composed of the inductor-pot system and one resonant capacitor. This state starts when  $S_H$  is triggered OFF. At this moment,  $D_L$  starts conducting and  $S_L$  can be triggered ON achieving ZVS switch-on conditions. This state finishes when  $S_L$  is deactivated, and the next state is state I.

The normalized differential equations system that defines the dynamics is

$$\frac{di_s(\theta)}{d\theta} = \frac{1}{\beta\omega_n Z_0} (V_s - v_{C_{rH}}(\theta)) \quad (19)$$

$$\frac{dv_{C_b}(\theta)}{d\theta} = \frac{Z_0}{\omega_n} \left( i_s(\theta) - i_0(\theta) \frac{2+\alpha}{\alpha} \right) \quad (20)$$

$$\frac{dv_{CrH}(\theta)}{d\theta} = \frac{Z_0}{\omega_n} (i_s(\theta)(1+\alpha) - i_0(\theta)\alpha) \quad (21)$$

$$\frac{dv_{CrL}(\theta)}{d\theta} = \frac{-Z_0}{\omega_n} (i_s(\theta)\alpha - i_0(\theta)(1+\alpha)) \quad (22)$$

$$\frac{di_0(\theta)}{d\theta} = \frac{1}{\omega_n Z_0} (v_{CrH}(\theta) - v_{Cb}(\theta) - R_{eq} \cdot i_0(\theta)). \quad (23)$$

The space state matrix for this state is shown in the next equation

$$\mathbf{A}_3 = \begin{pmatrix} 0 & 0 & \frac{-1}{\beta\omega_n Z_0} & 0 & 0 \\ \frac{Z_0}{\omega_n} & 0 & 0 & 0 & \frac{-Z_0(2+\alpha)}{\alpha\omega_n} \\ \frac{Z_0(1+\alpha)}{\omega_n} & 0 & 0 & 0 & \frac{-\alpha Z_0}{\omega_n} \\ \frac{-\alpha Z_0}{\omega_n} & 0 & 0 & 0 & \frac{Z_0(1+\alpha)}{\omega_n} \\ 0 & \frac{-1}{\omega_n Z_0} & \frac{1}{\omega_n Z_0} & 0 & \frac{-R_{eq}}{\omega_n Z_0} \end{pmatrix}$$

$$\mathbf{B}_3 = \begin{pmatrix} 1 \\ \beta\omega_n Z_0 \\ 0 \\ 0 \\ 0 \\ 0 \end{pmatrix}. \quad (24)$$

#### IV. SIMULATION RESULTS

By using the space-state analysis presented in Section III, two operating modes can be described (see Fig. 5). Both of them achieve ZVS switch-on conditions; however, only the first operation mode can achieve the ZVS switch-off conditions for  $S_H$ . The first operation mode uses the three states described earlier: I, II, and III. It makes possible to achieve ZVS conditions for the high-side switch in state II. The low-side switch has non-ZVS turn-off characteristic. However, turn-off current is always lower than in the high-side switch.

The second operation mode only uses two states: I and III. This operation mode does not achieve ZVS conditions during switch-off, and the switching losses are, therefore, increased. This switching losses can be reduced by using snubber capacitors [25], [26].

Nowadays, the induction heating appliances' power is limited by mains maximum current and voltage. The typical maximum output power is 3600 W, and the power converter prototype has been, therefore, designed to achieve 3600-W output power. Simulation parameters are  $C_r = 470$  nF, and the inductor is modeled by  $L_{eq} = 65$   $\mu$ H and 6.5  $\Omega$  for the series-equivalent resistor at switching frequency. The dc-link capacitor has been selected to be low enough to obtain a high power factor and a proper power control, as it is shown in this section, and it can be neglected in this analysis.

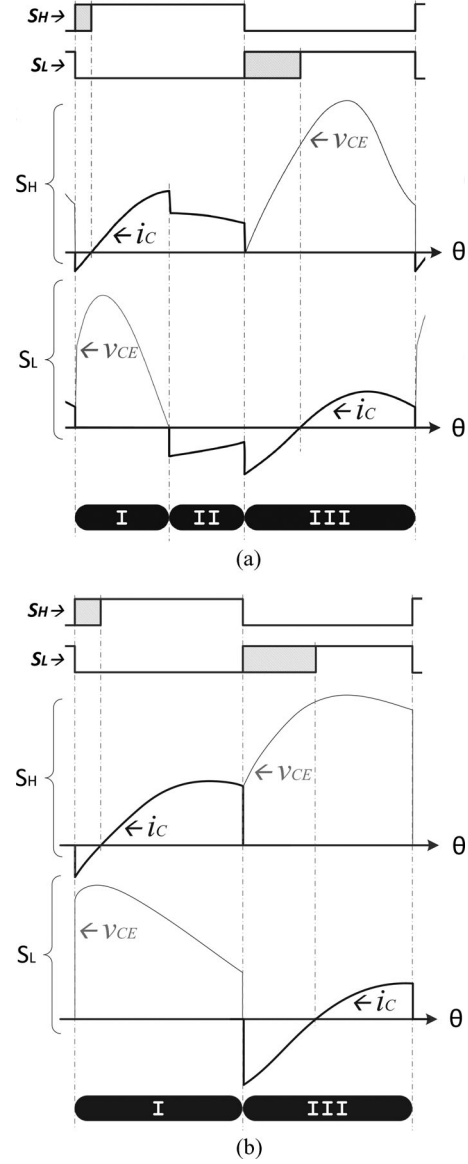


Fig. 5 Operation modes. (a) First operation mode. (b) Second operation mode.

The control strategies considered to control the output power are the square wave (SW) control, based on changing the switching frequency, and the asymmetrical duty cycle control [6], [25], [27], based on changing the duty cycle of the switching devices. Next subsections detail the main simulation results.

##### A. SW Control Review Stage

The SW control modifies the output power by controlling the switching frequency. The switching frequency is higher than the resonant frequency to achieve switch-on ZVS, and the output power is reduced when the switching frequency is increased (see Fig. 6).

As is shown in Fig. 6, the frequency range starts at 22 kHz, which is the resonant frequency determined by  $L_{eq}$  and  $C_r$ , that ensures ZVS switching-on conditions, and can be increased to decrease the output power. However, if the switching

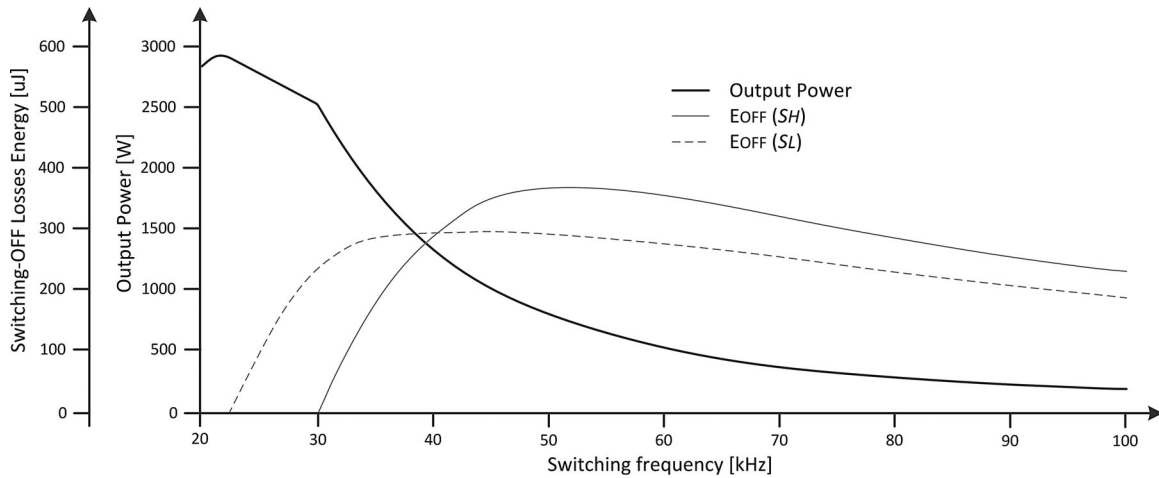


Fig. 6. SW control: output power and switching losses.

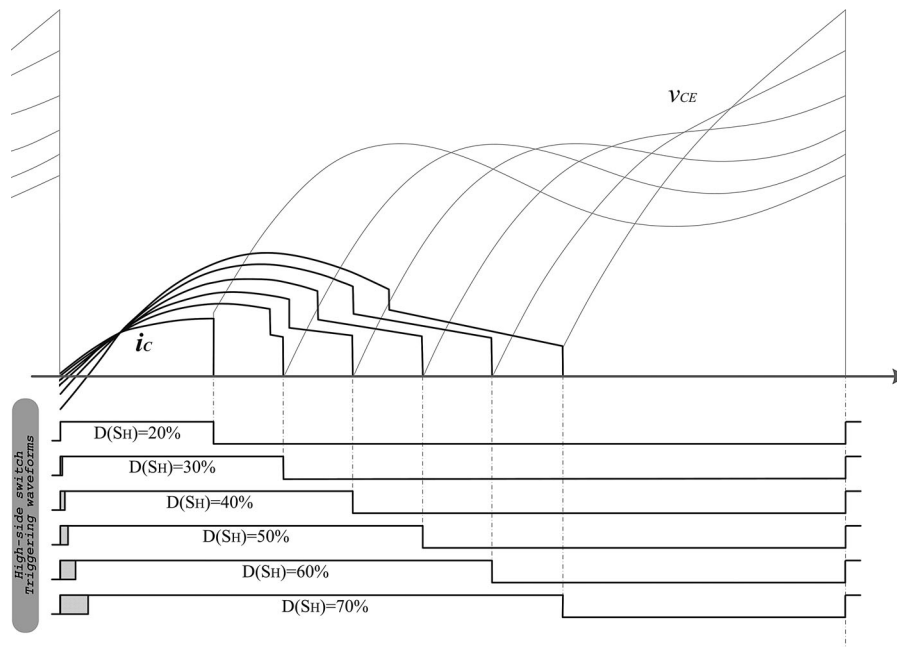


Fig. 7. ADC control strategy: main control signals and waveforms.

frequency reaches 30 kHz, switching-off losses increase because ZVS switching-off conditions are not achieved. As a result, the suitable switching frequency range and, therefore, the output power range is reduced. To overcome this limitation, the asymmetric duty cycle (ADC) control strategy is proposed.

### B. Asymmetrical Duty Cycle Control

The ADC control varies the output power by changing the switching device duty cycle. As is shown in Fig. 7, this control strategy delivers different output powers by changing the percent of conducting angle ( $\theta$ ) in which the high-side switch  $S_H$  is activated  $D(S_H)$ .

The low-side switch  $S_L$  conducting angle can be calculated as follows:

$$D(S_L) = 2\pi - D(S_H) - \theta_{DT} \quad (25)$$

where  $\theta_{DT}$  is the dead-time conducting angle to avoid short circuits. The variation of conducting angle is restricted by the achievement of soft-switching conditions for  $S_H$ , ZVS for switching-off, and by the achievement of ZVS in the switching-on commutation for both devices (antiparallel diode conduction at the beginning). In order to operate with switch-on ZVS conditions, the duty cycle must be higher than 30%. The upper boundary is kept to 60% to obtain a proper safety margin and balance the total amount of losses per switching device. Fig. 8 shows the power output variation achieved and the switching losses.

One of the key design aspects when designing the proposed converter to operate with the ADC control is the voltage that the switching devices must withstand. Fig. 9 shows the value of the voltage normalized to the input mains voltage as a function of the duty cycle for loads with (a) different  $Q_{eq}$  and (b) different

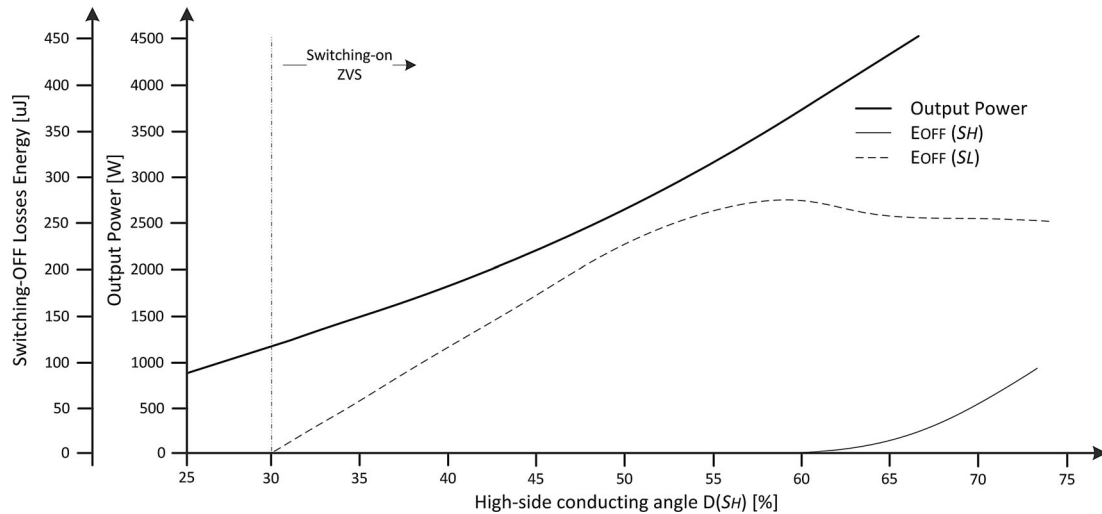


Fig. 8. Asymmetrical duty cycle control: output power and switching losses.

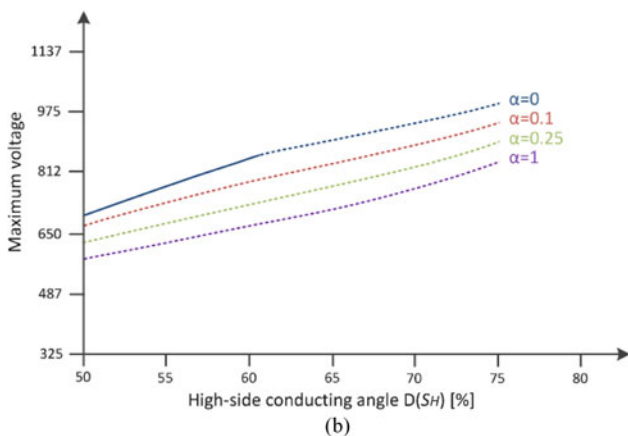
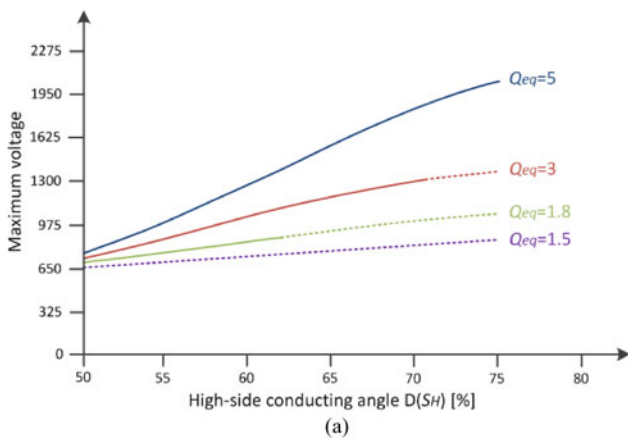


Fig. 9. Maximum voltage using 230 V rms supply voltage for different duty cycles: (a) values for different load quality factors and (b) values for different bus capacitors.

bus capacitors for the same  $Q_{eq}$ . In this figure, the optimum switching area is plotted with the solid line.

As is shown in Fig. 9(a), the induction load must be carefully designed to avoid unfeasible high voltages. Besides, Fig. 9(b) shows that the bus capacitor significantly reduces the duty cycle

TABLE I  
PROTOTYPE PARAMETERS

COMPONENTS	Values	
$L_{eq}$	Equivalent inductance	67 $\mu$ H
$R_{eq}$	Equivalent resistance	6.5 $\Omega$
$v_{ac,rms}$	Supply power source	230 V
$C_r$	Resonant capacitor	470 nF
$C_h$	DC-link capacitor	0 nF
$L_s$	Input inductance	1.4 mH
$R_s$	Equivalent series resistance	78 m $\Omega$
$S_{H, S_L}$	Switching device with anti-parallel diode	IGBT FGH30RN120
$D_{H, D_L}$	Rectifier diodes	DESP 60-12AR

operating range, whereas the voltage in the switching device is reduced. As a conclusion, for this design the bus capacitor is removed to improve the duty cycle operating range and, consequently, the output power control, and to reduce the number of components. However, other designs with lower output power control requirements may benefit of the voltage reduction.

As a conclusion, the output power in the proposed converter can be effectively controlled by means of SW and ADC control strategies. The output power can be reduced from the maximum value at the resonant frequency, 3000 W, to 1000 W without degrading the converter efficiency. If further reduction is required, pulse density modulation (PDM) [28] can be used to keep a high efficiency. The next section shows the main experimental results to validate the analytical and simulation results.

## V. EXPERIMENTAL RESULTS

To verify the proposed topology, a laboratory prototype was built. The desired maximum output power level is 3.6 kW, obtained at a switching frequency higher than 20 kHz to avoid the audible range. The inductor-pot system is characterized by  $R_{eq} = 6.5 \Omega$  and a measured equivalent inductance of 67  $\mu$ H. The measurements have been performed by means of a precision LCR meter from Agilent (E4980A). The power supply is fixed to 230 V and the input inductance  $L_s$  in this paper was set to 1.4 mH to avoid high-frequency ripple in the ac supply. The

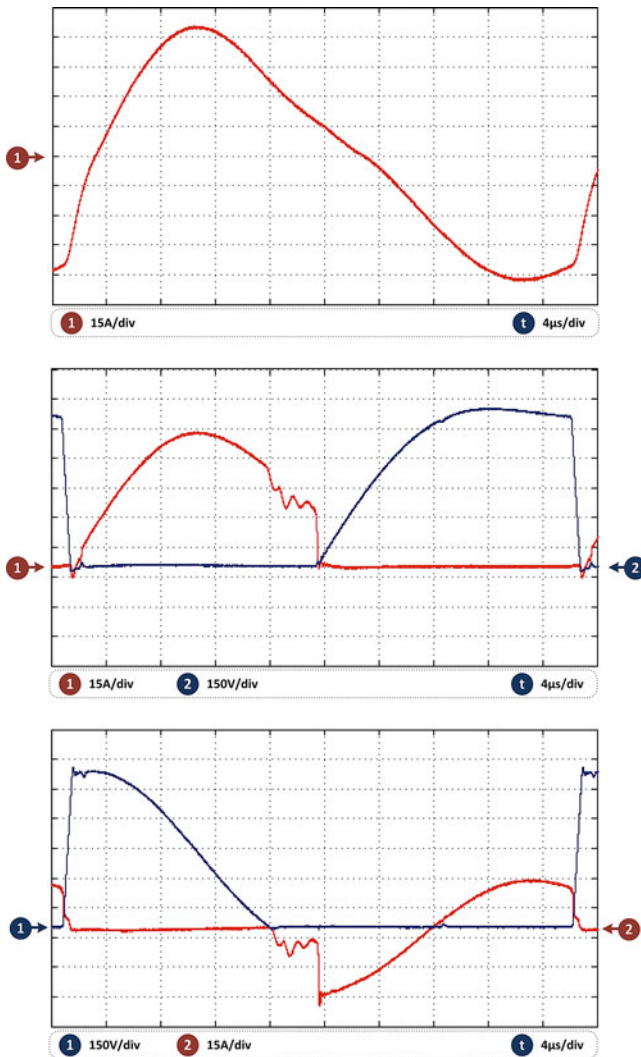


Fig. 10. Measured main waveforms. From top to bottom: inductor current (15 A/div), voltage (150 V/div), and current (15 A/div) in the high-side switch; and voltage (150 V/div) and current (15 A/div) in the low-side switch. Time: 4 μs/div.

control signals are generated by means of an FPGA-based digital pulsewidth modulator [29], [30]. Table I shows the component values for the prototype.

The main waveforms during a switching period for a 50% duty cycle are shown in Fig. 10, including the inductor current, and voltage and current through the switching devices. Besides, Fig. 11 shows the input voltage and current, and the load current during a mains half-cycle period. These measurements have been performed with an input inductor  $L_s = 1.4$  mH, considered in the measured efficiency. If further input current ripple reduction is required, either the power converter switching frequency or the input inductance can be increased. As a conclusion, these waveforms match up with the theoretical expected ones, and verify the proper operation of the converter.

The efficiency of the power converter has been measured using the power analyzer YOKOGAWA PZ-4000. The efficiency experimental results for both SW and ADC control strategies are shown in Fig. 12, where a comparison with the classical

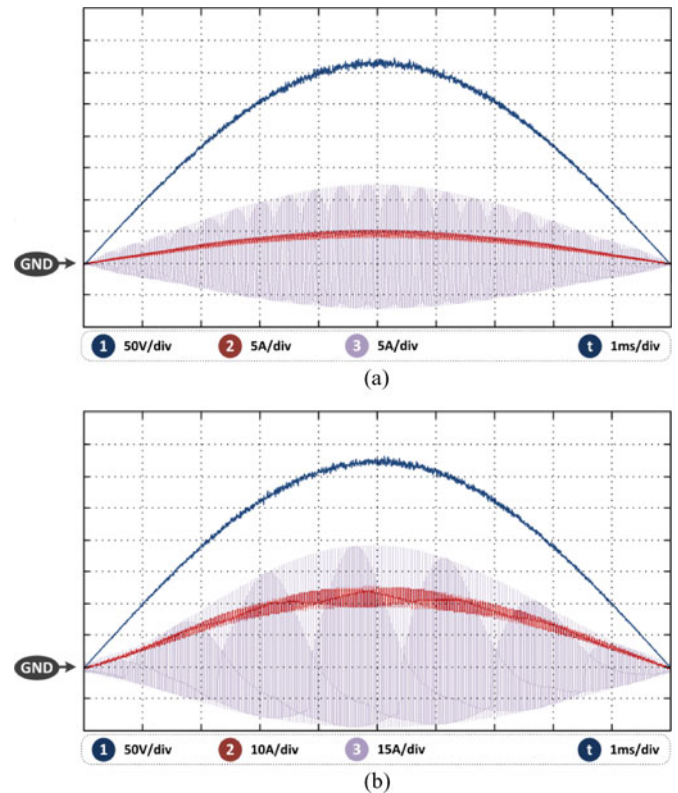


Fig. 11. Measured input waveforms for a mains half-cycle. (a) Maximum output power (3600 W; input voltage 50 V/div, input current 10 A/div, and load current 15 A/div). (b) Minimum output power (900 W; input voltage 50 V/div, input current and load current 5 A/div). Time: 1 ms/div.

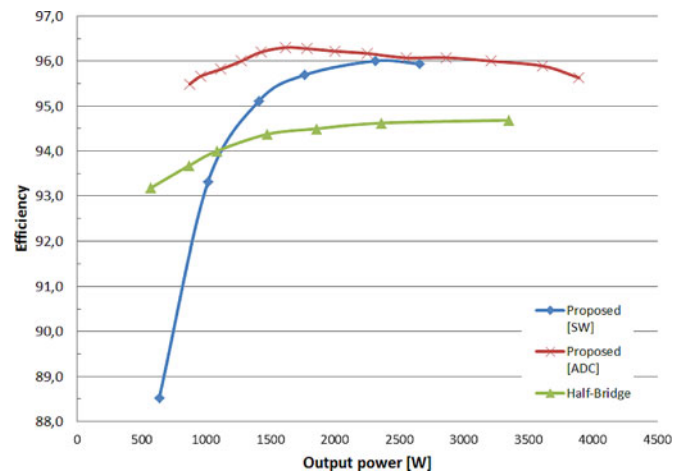


Fig. 12. Measured efficiency.

half-bridge topology [3]–[5] has been included. The classical topology has a reduced overvoltage and it is, therefore, implemented with 600-V HGTG20N60 IGBTs, whereas the proposed topology is implemented with 1200-V IGBTs. In spite of this, Fig. 11 shows that the proposed topology achieves a significant efficiency improvement in the whole operating range.

On one hand, the SW control strategy achieves a higher efficiency in the high-output power range. However, the efficiency significantly decreases in the low-output power range due to the switching losses. On the other hand, the ADC control achieves the same high efficiency in the high-output power range, but it remains constant due to the soft-switching conditions. It is important to note that the proposed topology with ADC control achieves a significant efficiency improvement compared with the classical half-bridge topology due to the power devices and current reduction and the soft-switching conditions.

## VI. CONCLUSION

This paper presents a new ac-ac converter applied to domestic induction heating. An analytical analysis has been performed in order to obtain the equations and operation modes that describe the proposed converter. The converter can operate with zero-voltage switching during both turn-on and turn-off commutations. Besides, the output voltage is doubled compared to the classical half-bridge, reducing the current through the switching devices. As a consequence, the power converter efficiency is improved in the whole operating range.

A 3.6-kW prototype has been designed and implemented in order to validate the analytical and simulation results. The experimental measurements show a significant efficiency improvement compared to the classical half-bridge topology and validate the feasibility of the proposed converter.

## REFERENCES

- [1] J. Acero, J. M. Burdío, L. A. Barragán, D. Navarro, R. Alonso, J. R. García, F. Monterde, P. Hernández, S. Llorente, and I. Garde, "Domestic induction appliances," *IEEE Ind. Appl. Mag.*, vol. 16, no. 2, pp. 39–47, Mar./Apr. 2010.
- [2] H. Fujita, N. Uchida, and K. Ozaki, "A new zone-control induction heating system using multiple inverter units applicable under mutual magnetic coupling conditions," *IEEE Trans. Power Electron.*, vol. 26, no. 7, pp. 2009–2017, Jul. 2010.
- [3] I. Millán, J. M. Burdío, J. Acero, O. Lucía, and S. Llorente, "Series resonant inverter with selective harmonic operation applied to all-metal domestic induction heating," *IET Power Electron.*, vol. 4, pp. 587–592, May 2011.
- [4] R. L. Steigerwald, "A comparison of half-bridge resonant converter topologies," *IEEE Trans. Power Electron.*, vol. 3, no. 2, pp. 174–182, Apr. 1988.
- [5] H. W. Koertzen, J. D. van Wyk, and J. A. Ferreira, "Design of the half-bridge series resonant converters for induction cooking," in *Proc. IEEE Power Electron. Spec. Conf. Records*, 1995, pp. 729–735.
- [6] H. Pham, H. Fujita, K. Ozaki, and N. Uchida, "Phase angle control of high-frequency resonant currents in a multiple inverter system for zone-control induction heating," *IEEE Trans. Power Electron.*, vol. 26, no. 11, pp. 3357–3366, Nov. 2011.
- [7] W. Yunxiang, M. A. Shafi, A. M. Knight, and R. A. McMahon, "Comparison of the effects of continuous and discontinuous PWM schemes on power losses of voltage-sourced inverters for induction motor drives," *IEEE Trans. Power Electron.*, vol. 26, no. 1, pp. 182–191, Jan. 2011.
- [8] I. Takahashi, "Power factor improvement of a diode rectifier circuit by dither signals," in *Conf. Record IEEE Ind. Appl. Soc. Annu. Meet.*, 1990, pp. 1289–1294.
- [9] A. A. Boora, A. Nami, F. Zare, A. Ghosh, and F. Blaabjerg, "Voltage-sharing converter to supply single-phase asymmetrical four-level diode-clamped inverter with high power factor loads," *IEEE Trans. Power Electron.*, vol. 25, no. 10, pp. 2507–2520, Oct. 2010.
- [10] L. Meng, K. Cheng, and K. Chan, "Systematic approach to high-power and energy-efficient industrial induction cooker system: Circuit design, control strategy and prototype evaluation," *IEEE Trans. Power Electron.*, vol. 26, no. 12, pp. 3754–3765, Dec. 2011.
- [11] N. Nguyen-Quang, D. A. Stone, C. M. Bingham, and M. P. Foster, "Single phase matrix converter for radio frequency induction heating," in *Proc. IEEE Int. Symp. Power Electron., Electr. Drives, Autom. Motion*, May, 2006, pp. 614–618.
- [12] N. Nguyen-Quang, D. A. Stone, C. Bingham, and M. P. Foster, "Comparison of single-phase matrix converter and H-bridge converter for radio frequency induction heating," in *Proc. Eur. Conf. Power Electron. Appl.*, 2007, pp. 1–9.
- [13] O. Lucía, F. Almazán, J. Acero, J. M. Burdío, and C. Carretero, "Multiple-output resonant matrix converter for multiple-inductive-load systems," in *Proc. IEEE Appl. Power Electron. Conf. Expo.*, 2011, pp. 1338–1343.
- [14] L. Gang, S. Kai, H. Lipei, and I. Seiki, "RB-IGBT gate drive circuit and its application in two-stage matrix converter," in *Proc. IEEE Appl. Power Electron. Conf. Expo.*, 2008, pp. 245–251.
- [15] H. Sugimura, S.-P. Mun, S.-K. Kwon, T. Mishima, and M. Nakaoka, "High-frequency resonant matrix converter using one-chip reverse blocking IGBT-based bidirectional switches for induction heating," in *Proc. IEEE Power Electron. Spec. Conf.*, 2008, pp. 3960–3966.
- [16] C. Aguilar, A. Ruiz, F. Canales, and F. Lee, "Analysis of the half-bridge boost rectifier as integrated electronic ballast with power factor correction," in *Proc. IEEE Power Electron. Spec. Conf.*, 2001, pp. 707–712.
- [17] N. A. Ahmed and M. Nakaoka, "Boost-half-bridge edge resonant soft switching PWM high-frequency inverter for consumer induction heating appliances," *IEE Proc. Electr. Power Appl.*, vol. 153, no. 6, pp. 932–938, Nov. 2006.
- [18] H. L. Cheng, C. S. Moo, and W. M. Chen, "A novel single-stage high-power-factor electronic ballast with symmetrical topology," *IEEE Trans. Ind. Electron.*, vol. 50, no. 4, pp. 759–766, Aug. 2003.
- [19] W. Chien-Ming, "A novel single-stage high-power-factor electronic ballast with symmetrical half-bridge topology," *IEEE Trans. Ind. Electron.*, vol. 55, no. 2, pp. 969–972, Feb. 2008.
- [20] R. N. do Prado, M. F. da Silva, M. Jungbeck, and A. R. Seidel, "Low cost high-power-factor electronic ballast for compact fluorescent lamps," in *Proc. IEEE Ind. Appl. Conf.*, 1999, pp. 256–261.
- [21] A. Ruiz, C. Aguilar, and J. Arau, "Half-bridge boost rectifier as power factor corrector-electronic ballast [ballast read ballast]," in *IEEE Power Electron. Congr.*, 2000, pp. 136–141.
- [22] K. Chong-Eun, M. Gun-Woo, and H. Sang-Kyoo, "Voltage doubler rectified boost-integrated half bridge (VDRBHB) converter for digital car audio amplifiers," *IEEE Trans. Power Electron.*, vol. 22, no. 6, pp. 2321–2330, Nov. 2007.
- [23] A. Fujita, H. Sadakata, I. Hirota, H. Omori, and M. Nakaoka, "Latest developments of high-frequency series load resonant inverter type built-in cooktops for induction heated all metallic appliances," in *IEEE Power Electron. Motion Control Conf.*, 2009, pp. 2537–2544.
- [24] J. Acero, C. Carretero, I. Millán, O. Lucía, R. Alonso, and J. M. Burdío, "Analysis and modeling of planar concentric windings forming adaptable-diameter burners for induction heating appliances," *IEEE Trans. Power Electron.*, vol. 26, no. 5, pp. 1546–1558, May 2011.
- [25] O. Lucía, J. M. Burdío, I. Millán, J. Acero, and L. A. Barragán, "Efficiency oriented design of ZVS half-bridge series resonant inverter with variable frequency duty cycle control," *IEEE Trans. Power Electron.*, vol. 25, no. 7, pp. 1671–1674, Jul. 2010.
- [26] O. Lucía, C. Carretero, D. Palacios, D. Valeau, and J. M. Burdío, "Configurable snubber network for efficiency optimization of resonant converters applied to multi-load induction heating," *Electron. Lett.*, vol. 47, no. 17, pp. 989–991, Aug. 2011.
- [27] J. Kim, H. S. Song, and K. Nam, "Asymmetric duty control of a dual-half-bridge dc/dc converter for single-phase distributed generators," *IEEE Trans. Power Electron.*, vol. 26, no. 3, pp. 973–982, May 2011.
- [28] O. Lucía, J. M. Burdío, I. Millán, J. Acero, and D. Puyal, "Load-adaptive control algorithm of half-bridge series resonant inverter for domestic induction heating," *IEEE Trans. Ind. Electron.*, vol. 56, no. 8, pp. 3106–3116, Aug. 2009.
- [29] D. Navarro, O. Lucía, L. A. Barragán, J. I. Artigas, and O. Jiménez, "Synchronous FPGA-based implementations of digital pulse width modulators," *IEEE Trans. Power Electron.*, vol. 27, no. 5, pp. 2515–2525, May 2012.
- [30] O. Lucía, L. A. Barragán, J. M. Burdío, O. Jiménez, D. Navarro, and I. Urriza, "A versatile power electronics test-bench architecture applied to domestic induction heating," *IEEE Trans. Ind. Electron.*, vol. 58, no. 3, pp. 998–1007, Mar. 2011.





**Héctor Sarnago** (M'09) received the M.Sc. degree in electrical engineering from the University of Zaragoza, Zaragoza, Spain, in 2010, where he is currently working toward the Ph.D. degree.

His main research interests include resonant converters and digital control for induction heating applications.

Mr. Sarnago is a member of the Aragon Institute for Engineering Research (I3A).



**Óscar Lucía** (S'04–M'11) received the M.Sc. and Ph.D. degrees in electrical engineering from the University of Zaragoza, Zaragoza, Spain, in 2006 and 2010, respectively.

He is currently an Assistant Professor in the Department of Electronic Engineering and Communications, University of Zaragoza. His main research interests include multiple output converters, digital control, and resonant power conversion for induction heating applications.

Dr. Lucía is a member of the Aragon Institute for Engineering Research (I3A).



**Arturo Mediano** (SM'06) received the M.Sc. and Ph.D. degrees in electrical engineering from the University of Zaragoza, Zaragoza, Spain, in 1990 and 1997, respectively.

Since 1992 he has been involved in a teaching professorship with special interests in RF (HF/VHF/UHF) and EMI/EMC design for Telecom and Electrical Engineers. Since 1990, he has been involved in design and management responsibilities for research and development projects in the RF field for communications, industry, and scientific applications.

His research interest includes high-efficiency switching-mode RF power amplifiers where he has experience in applications such as broadcast, mobile communication radios, through-earth communication systems, induction heating, plasmas for industrial applications, and RF identification. He has an experience in collaboration with industry (including training and consultancy in RF and electromagnetic interference/electromagnetic compatibility).

Dr. Mediano is an active member from 1999, now ViceChair, of the MTT-17 (HF/VHF/UHF technology) Technical Committee of the Microwave Theory and Techniques Society of the IEEE.